

Correlated X-ray/UV/optical emission and short term variability in a Seyfert 1 galaxy NGC 4593

Main Pal* & Sachindra Naik †

Astronomy and Astrophysics Division, Physical Research Laboratory, Ahmedabad - 380009, India

20 August 2019

ABSTRACT

We present a detailed multi-frequency analysis of an intense monitoring programme of Seyfert 1 galaxy NGC 4593 over a duration of nearly for a month with *Swift* observatory. We used 185 pointings to study the variability in six ultraviolet/optical and two soft (0.3–1.5 keV) and hard X-ray (1.5–10 keV) bands. The amplitude of the observed variability is found to decrease from high energy to low energy (X-ray to optical) bands. Count-count plots of ultraviolet/optical bands with hard X-rays clearly suggest the presence of a mixture of two major components: (i) highly variable component such as hard X-ray emission and (ii) slowly varying disc-like component. The variations observed in the ultraviolet/optical emission are strongly correlated with the hard X-ray band. Cross-correlation analysis provides the lags for the longer wavelengths compared to the hard X-rays. Such lags clearly suggest that the changes in the ultraviolet/optical bands follow the variations in the hard X-ray band. This implies the observed variation in longer wavelengths is due to X-ray reprocessing. Though, the measured lag spectrum (lag vs. wavelength) is well described by $\lambda^{4/3}$ as expected from the standard disc model, the observed lags are found to be longer than the predicted values from standard disc model. This implies that the actual size of the disc of NGC 4593 is larger than the estimated size of standard thin disc as reported in AGN such as NGC 5548, Fairall 9.

Key words: accretion, accretion disc–galaxies: active, galaxies: individual: NGC 4593, galaxies: nuclei, X-rays: galaxies

1 INTRODUCTION

Active galactic nuclei (AGN) are normally considered to have accreting supermassive black holes (SMBHs) at the heart of the host galaxies. The radiation from these AGN covers almost entire range of electromagnetic spectrum – starting from X-ray to Radio bands. The X-ray continuum emission from these objects are considered to be dominated by the power law model which is known to be due to the inverse Compton scattering of soft photons in an optically thin i.e., $\tau \sim 1$ and hot electron plasma i.e., $kT_e \sim 100\text{keV}$ (Sunyaev & Titarchuk 1980; Haardt & Maraschi 1991). The soft photons observed in these sources are believed to be emitted from the accretion disc around the SMBH. The accretion disc, as proposed by Shakura & Sunyaev (1973), is assumed to be geometrically thin and optically thick. In the accretion disc, the energy loss due to the viscous heating is being emitted as blackbody emission corresponding to the temperature at a given radius. The temperature at a certain distance from the center is inversely proportional to the three–fourth power of the distance. Depending on the temperature, the disc emits radiation in the range of ultraviolet (UV)

to optical bands (Koratkar & Blaes 1999; Yuan & Narayan 2014). However, sometimes the inner disc becomes sufficiently hot and partly contributes at the soft X-ray band (e.g., Boller et al. 1996; Leighly 1999).

In Seyfert galaxies, radiation emitted from the accretion disc is dominated in UV band. However, due to large Galactic absorption along the line of sight, the UV radiation peak is hardly detectable. The observed UV/optical emission show different variabilities on various timescales from days to years for $10^{6-9} M_\odot$ black hole mass range (e.g., Arévalo et al. 2008; Mehdipour et al. 2011; McHardy et al. 2014; Shappee et al. 2014; McHardy et al. 2016). However, the cause of observed variabilities in UV/optical emission from the accretion disc is not very clear. The observed UV/optical emission variabilities in Seyfert galaxies are thought to be associated with the fluctuation in the mass accretion (Marshall et al. 2008; Arévalo et al. 2008). However, such interpretation is unable to explain the observed disc variability on short (hours to days) timescale. This variability timescale is very much shorter compared to the expected timescale of the density fluctuations in the accretion flow. The variations observed in X-ray emission are found to lead the variations in UV/optical band (Shappee et al. 2014; McHardy et al. 2014). This is difficult to ex-

* Email: mainpal@prl.res.in

†

plain by using the hypothesis that the cause of UV/optical variation is associated with accretion flow fluctuation.

Krolik et al. (1991) suggested that the fluctuations occurring in the UV/optical radiation are delayed compared to the X-ray emission if the variations in the X-ray band lead the changes in UV/optical band. This occurs when the X-ray radiation from the compact corona around the SMBH illuminates the optically thick disc and gets absorbed and reprocessed into the UV/optical radiation. The predicted delay in the reprocessed UV/optical radiation with respect to the X-ray radiation varies as the 4/3rd power of wavelength i.e. $\tau \propto \lambda^{4/3}$ (Collier et al. 1999; Cackett et al. 2007). Such prediction of lags have been detected in the multi-frequency study of several AGN (Cackett et al. 2007; Breedt et al. 2010; McHardy et al. 2014; Troyer et al. 2016; Edelson et al. 2015; Fausnaugh et al. 2016; Buisson et al. 2017; Edelson et al. 2017). On the other hand, Gaskell (2008) found that the fluctuations in the UV/optical radiation are independent of the variations in X-rays. It is proposed that the origin of these fluctuations in both the bands are likely to be local to the disc. Occasionally, rapid changes are found in the optical radiation compared to that of the X-ray radiation suggesting distinct regions for their origin (e.g., NGC 3783; Arévalo et al. 2009).

Multi-frequency observation campaign of AGN provide an opportunity to investigate different regions of the central engine. Till the launch of *XMM-Newton*, only a few contemporaneous long and intensive multi-frequency campaigns were carried out. Monitoring programs with the space-based *RXTE* observatory and ground-based telescopes were carried out for a few AGN (e.g., Maoz et al. 2002; Arévalo et al. 2008, 2009; Breedt et al. 2010). At present, there are excellent space-based observatories i.e., *XMM-Newton*, *Swift* and *ASTROSAT* which have the capabilities to carry out simultaneous multi-band observations in the UV/optical and X-ray bands. A number of Seyfert 1 galaxies have revealed strong correlation between the UV/optical and the X-ray bands (Mehdipour et al. 2011; McHardy et al. 2014; Troyer et al. 2016; Edelson et al. 2015; Noda et al. 2016; Buisson et al. 2017; Lobban et al. 2017; Edelson et al. 2017; Pal et al. 2017a; Starkey et al. 2017; Noda et al. 2016; Connolly et al. 2016; McHardy et al. 2016; Fausnaugh et al. 2016). In some cases, a relatively moderate correlation have been observed between UV/optical and X-ray bands (e.g., NGC 7469: Nandra et al. 1998). However, a few AGN have shown no clear connection in the UV/optical and the X-ray emission (Maoz et al. 2002; Pal et al. 2016). Thus, the correlation and variations between the UV/optical emission and the X-ray emission are complex and their intensive exploration is required.

To investigate the cause of variation in emitted radiation from different parts of the accretion disc, multi-band monitoring observations of Seyfert 1 galaxy NGC 4593 with *Swift* observatory have been used in the present study. This AGN is a barred Seyfert 1 galaxy, classified as Hubble type SBb, located at a redshift of $z = 0.009$ (Strauss et al. 1992). This AGN is mildly X-ray luminous with $2 - 10\text{keV}$ luminosity $L_{2-10\text{keV}} \sim 10^{42} \text{ erg s}^{-1}$ (Ebrero et al. 2013) and harbors a supermassive black hole of mass $\sim (1 - 10) \times 10^6 M_{\odot}$ (Denney et al. 2006; Peterson et al. 2004; Onken et al. 2003; Gebhardt et al. 2000). NGC 4593 has been found to be highly variable in X-ray, UV, optical and infrared (IR) bands, suggesting the emitting region to be a compact source at the centre (Santos-Lleo et al. 1995; Ursini et al. 2016). Previous studies revealed the absence of broad iron $K\alpha$ line in the X-ray spectrum, instead two narrow lines at 6.4 keV and 6.97 keV have been detected (Brenneman et al. 2007; Markowitz & Reeves

2009). Markowitz & Reeves (2009) suggested that the accretion disc may be truncated at some inner region with radiatively inefficient flow while the outer disc remains radiatively efficient. However, Reynolds et al. (2004) discussed the lack of relativistic iron $K\alpha$ line is possibly due to the low iron abundance, highly ionized surface and high inclination of the disc. They inferred that the radiatively efficient accretion disc is consistent and can be extended down to the inner most stable radius. In this work, we explore various regions of the accretion disc and its coupling with the X-ray continuum by using multi-frequency observations with *Swift* observatory.

In the paper, we discuss the observation and the data reduction in Section 2. UV/optical and X-ray light curves analysis and related cross-correlation studies are described in Section 3. We list our findings and discuss the results in Section 4.

2 OBSERVATIONS AND DATA REDUCTION

We used *Swift*/Ultraviolet/Optical Telescope (UVOT) (Romig et al. 2005) and *Swift*/X-ray Telescope (XRT) (Burrows et al. 2005) archival data of the AGN from 2016 July 13 to 2016 August 5 in our analysis. Both the instruments are simultaneously used during observations providing coverages in X-ray and UV/optical bands.

Data obtained from UVOT observations, contemporaneous to that of XRT, were reduced by following standard procedure. We used sky image files, free from any change in the source position, to get the count rate for each filter of every observation. We summed available multiple frame exposures by using `UVOTIMSUM` to increase the signal to noise ratio. A circular region of radius 5 arcsec centred at source coordinate was selected to extract the spectrum for all filters of each observation. Annular regions with inner and outer radii of 100 and 120 arcsec, respectively, with source at the centre were selected for background estimation for all the observations (see Fig. 1). The background region is carefully selected to avoid the contribution from extended components in the galaxy. `UVOTSOURCE` package was used internally by `UVOT2PHA` task to compute the source count rate by using latest calibration files¹. Following above procedure, source and background spectral products were extracted for each observation. Background corrected source count rates for all the filters were estimated for every observation. We also checked small scale sensitivity (SSS) by running `UVOTSOURCE` on sky images of all the filters using latest SSS file². The data points which landed on the low sensitivity patches of the CCD are marked with crosses and are shown in the left panels of Fig. 2. Apart from this, there are very few data points, marked with asterisk in the left panels of Fig. 2, which show $\geq 15\%$ variability compared to the local mean. This variability might be caused due to the tracking of telescope as quoted in McHardy et al. (2014). We excluded all these data points marked with crosses and asterisks in the figure from our analysis. This resulted in a total of 160 to 184 usable data points (average count rates) for UVOT filters.

As described in Evans et al. (2007, 2009), *Swift*/XRT product generator³ online software package was used to extract source light curves. On-target exposure of every pointing was about 1 ks (Table 1). For each monitoring epoch, average count rate over entire duration of observation was extracted from photon counting

¹ <https://heasarc.gsfc.nasa.gov/ftools/caldb/help/uvot2pha.html>

² https://swift.gsfc.nasa.gov/analysis/uvot_digest/sss_check.html

³ http://www.swift.ac.uk/user_objects/

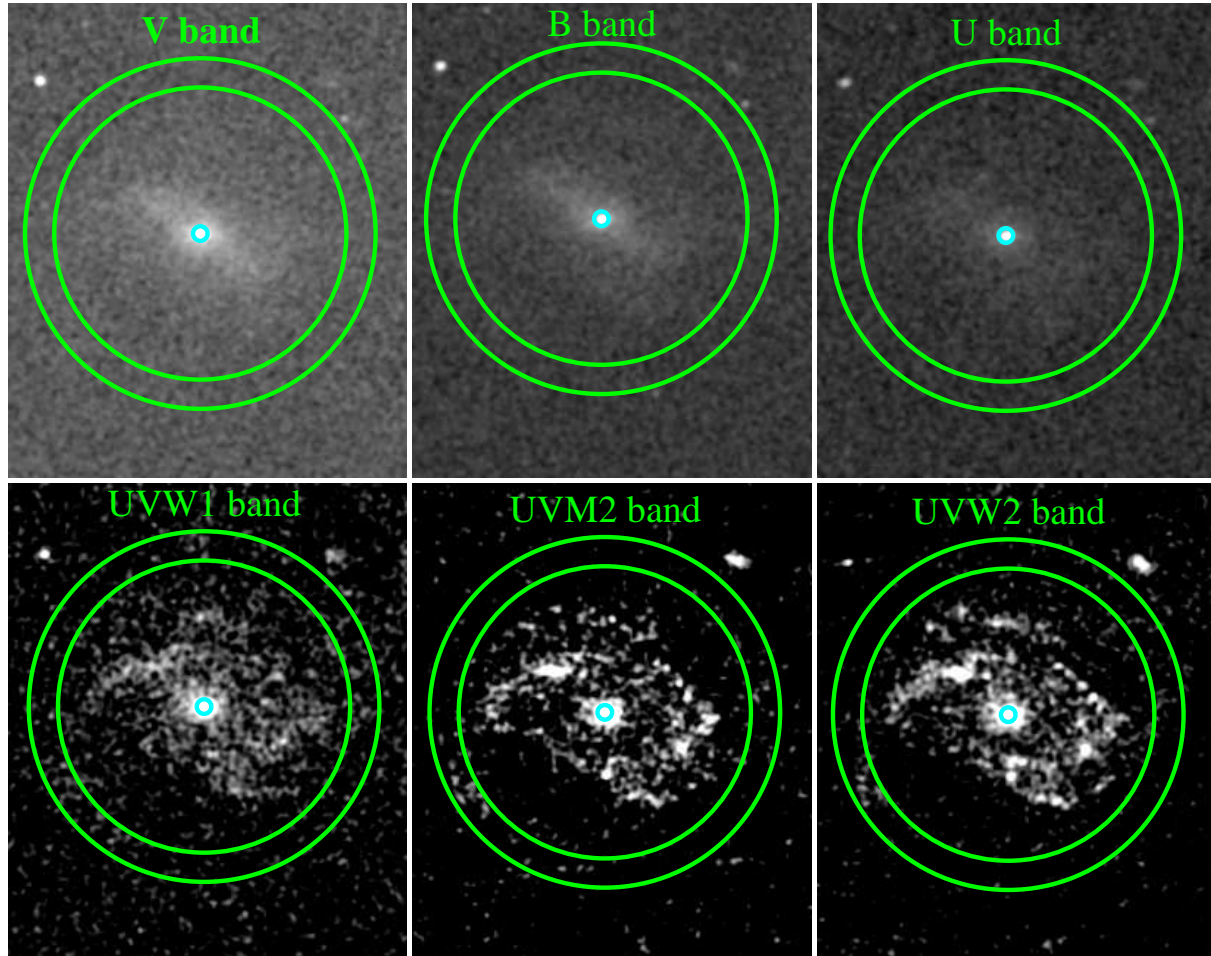


Figure 1. In all the UV/optical bands, the nucleus is located at the centre. The extended emission with bar-like structure is clearly visible in the optical bands (top panels) while the arm like structure of the galaxy NGC 4593 appears only in UV bands (bottom panels). Source and background regions used to extract UV/optical light curves from an epoch of observation (Image shown for ID : 00092353198) are shown in each panel. Upper panels show the selection of regions from V to U-band whereas lower panels show for UVW1 to UVW2 bands.

(PC) mode of XRT. We found a total of 185 usable data points for our study (see right panel of Fig. 2). For spectral study, we used XRTPIPELINE to extract event files incorporating the latest calibration data base. This tool selects a circular region of radius 20 pixels (~ 47 arcsec) centred at the source co-ordinates to extract source spectrum. We also created background spectrum using an annular region with inner and outer radii of 20 and 45 pixels, respectively, centred at the source co-ordinates. Since PC mode data sets are affected by pile-up in our case, we removed the circular core of point spread function (PSF) of radius in the range 2 to 4 pixels as recommended by instrument team to mitigate the effect. We also generated the effective area file by using XRTMKARF. We grouped the source spectrum to get a minimum of 15 counts per bin to make use of χ^2 minimization technique.

3 DATA ANALYSIS

3.1 Count–Count Correlation with Positive Offset (C3PO)

The 1.5–10 keV and 0.3–1.5 keV bands light curves for the entire duration of monitoring campaign were created by using observed average count rates for each epoch of observation. In our analysis, the 1.5–10 keV band stands for the hard X-ray band where

Table 1. Log of observation of NGC 4593 with *Swift* XRT/UVOT

Observation ID	00092353001–00092353201
Date of Observations	2016 July 13 - 2016 August 5
MJD	57582.8 - 57605.4
No. of IDs for XRT	185
No. of IDs for UVOT	160-184

power-law continuum is thought to be the primary component. The 0.3–1.5 keV band stands for the soft X-ray band which may contain a complex mixture of multiple spectral components such as due to warm absorption along the line of sight, blurred reflection from partially ionized disc and possible intrinsic disc Comptonization. In right panel of Fig. 2, the hard X-ray light curve, the soft X-ray light curve and their ratio (1.5-10 keV/0.3-1.5 keV) are shown for all observations from 2016 July 13 to 2016 August 5. It can be seen from the figure that the both soft and hard X-ray emission vary about five times on a few week timescale and vary by a factor of ~ 2 on short (a few hours) timescale. The hardness ratio appears almost constant during the entire monitoring duration while it seems to vary rapidly on a few hours timescale. Similarly, we found that UV and optical emission are also highly variable and each light curve appears to

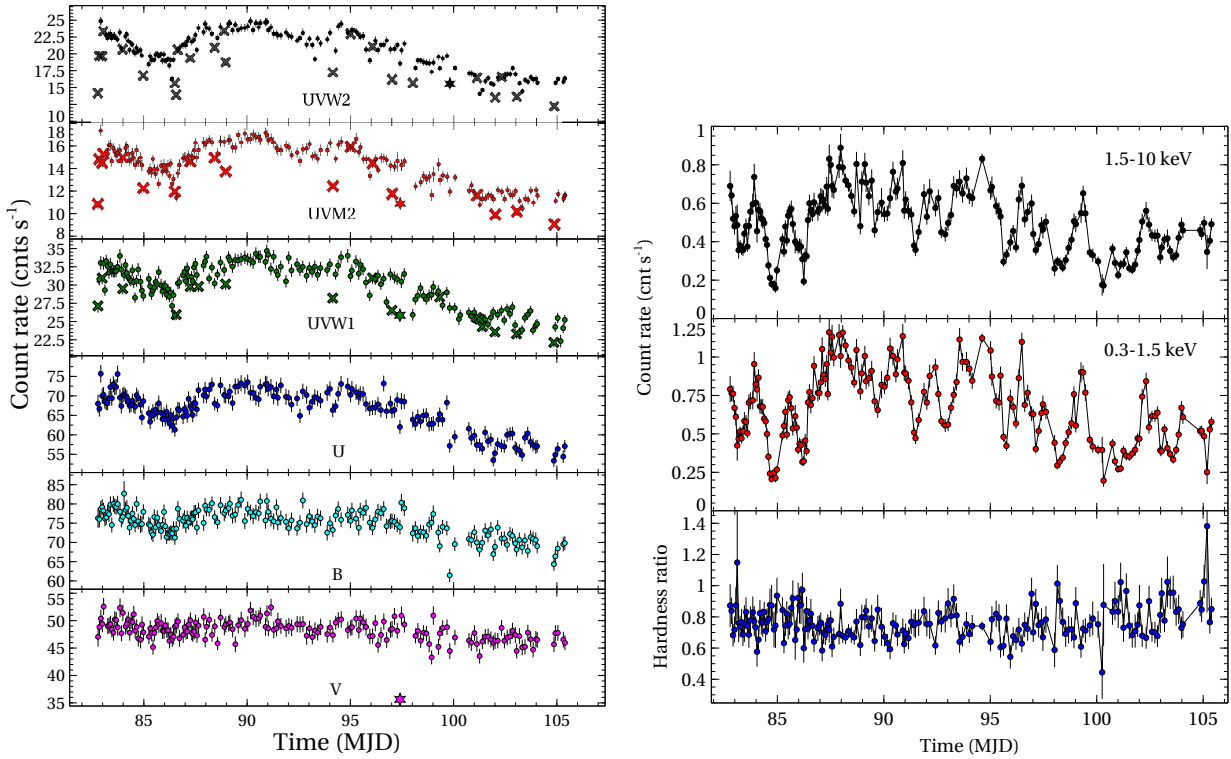


Figure 2. Left panels : UV (UVW2, UVM2, UVW1 and U bands) and optical (B and V bands) light curves, simultaneous to X-ray light curves are presented from top to bottom panels. Right panels : Light curves in 1.5 – 10 keV (top panel), 0.3 – 1.5 keV (middle panel) ranges and hardness ratio i.e., 1.5 – 10 keV/0.3 – 1.5 keV (bottom panel) are shown. The time axis is in MJD-57500.

be correlated to each other. Further, the hardness ratio and hard X-ray count rate seem anti-correlated suggesting this AGN retains its nature being softer when brighter as shown in Fig. 3 (Ursini et al. 2016).

We fitted each pair of soft band (soft X-ray, UVW2, UVM2, UVW1, U, B and V) and hard X-ray band with a line $y = m \times x + c$, where m and c are slope and offset. The slope m tells about how strongly y depends on x , while the offset c provides information about the slowly varying component as discussed by Noda et al. (2013a,b, 2011). This method is known as count-count correlation with positive offset (C3PO). Such a method was first developed by Churazov et al. (2001) in a binary system Cygnus X-1 to decompose the stable and variable components. Later, Taylor et al. (2003) applied above method on AGN. We used hard X-ray band as the abscissa (e.g., x) and any soft band as the ordinate (e.g., y). After linear function fitting to the pair of a soft band and hard X-ray band, we found that the soft X-ray consists of a negative offset (-0.08 ± 0.02) while other UV/optical bands have positive offset (e.g., $\sim 9 - 57$). The marginal negative offset for soft X-ray band suggests that this band is possibly affected by absorption as reported in previous studies (e.g., Ursini et al. 2016; Ebrero et al. 2013). The positive offset for UV/optical emission hints a presence of weakly varying component such as disc emission. The positive slopes (e.g., $\sim 1.5 - 24$) indicate a strong relationship between soft bands and hard X-ray band as shown in count-count plots of Fig. 4). However, the linear fit is not enough to describe all bands due to the scatters around the fitted line except the soft X-ray and V bands (see Fig. 4).

The possible cause of these scatters can be due to the contributions from the broad line regions (BLR) and narrow line regions

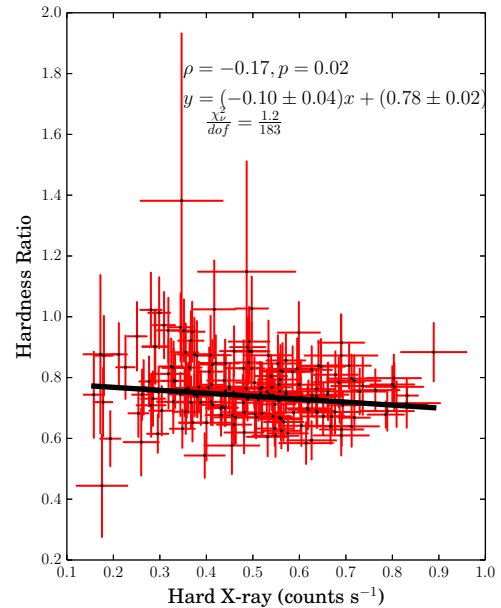


Figure 3. The correlation between hardness ratio and hard X-ray count rate is shown. This provides an anti-correlation which suggests that this source is softer when brighter.

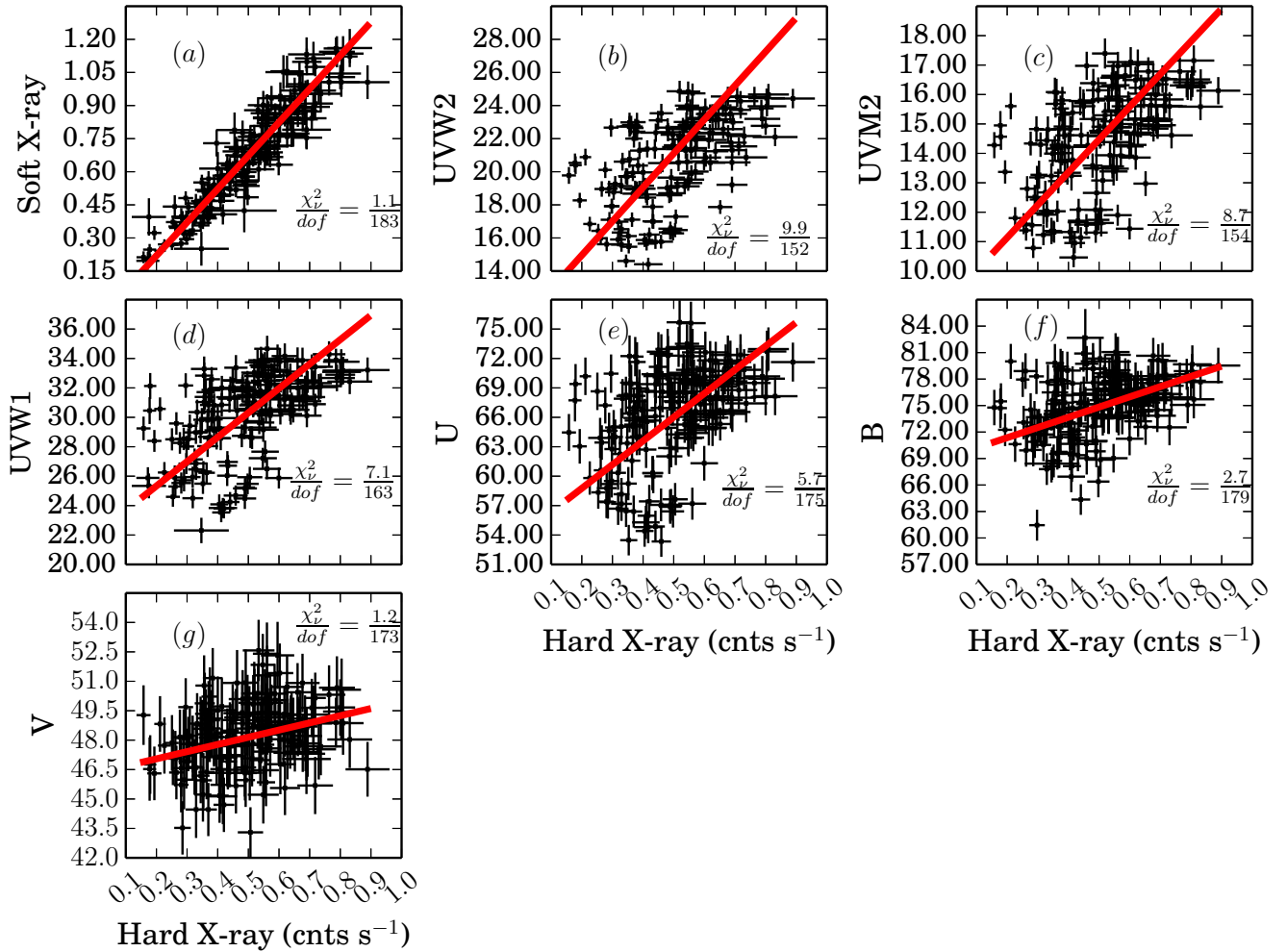


Figure 4. Count-count plots between different bands are shown. The linear fittings ($y=m \times x+c$, where m and c are slope and offset, respectively) to the correlation between soft bands (soft X-ray to V bands) and the hard X-ray band are shown as solid lines. The best-fit linear equation obtained from modeling are (a) $y = (1.51 \pm 0.03)x + (-0.08 \pm 0.02)$ (b) $y = (20.5 \pm 1.8)x + (10.9 \pm 0.8)$ (c) $y = (11.1 \pm 1.0)x + (8.9 \pm 0.5)$ (d) $y = (16.6 \pm 1.5)x + (22.0 \pm 0.7)$ (e) $y = (24.2 \pm 0.26)x + (53.9 \pm 1.3)$ (f) $y = (11.6 \pm 1.6)x + (69.0 \pm 0.8)$ (g) $y = (3.7 \pm 0.8)x + (46.3 \pm 0.4)$. In each panel, the count rates used are in the unit of counts s^{-1} .

(NLR) of the host galaxy. An estimate of the fractional contribution due to the emission lines from the BLR and NLR can be made by taking the ratio between the net equivalent widths of the lines in the band and the full width at half maximum (FWHM) of the filter. We used equivalent widths of all narrow and broad emission lines from Vanden Berk et al. (2001) in UVW2, UVM2, UVW1, U, B and V bands and obtained the net equivalent widths in each band. We also obtained the FWHM for each band from Poole et al. (2008). We then divided the net equivalent width of all the lines in each band by the respective FWHM. We found the resultant fraction to be $\sim 3.5\%$ in V band, $\sim 9\%$ in B band, $\sim 1.2\%$ in U band, $\sim 5.5\%$ in UVW1 band, $\sim 1.6\%$ in UVM2 band and $\sim 4.1\%$ in UVW2 band. These fractions clearly suggest that the total emission in various bands are affected from BLR/NLR components of the host galaxy.

3.2 Time lag estimation

We used Pearson's correlation coefficient ' ρ ' to quantify the strength of inter-band correlation (soft band and hard X-ray light curves). We also determined the significance of the strength of correlation between longer wavelength bands and hard X-ray band. We obtained the correlation coefficient ' ρ ' to be within $\sim \rho = 0.29$ and $\rho \sim 0.94$ from optical/UV to soft X-ray bands with very low probability p ($\sim p = 1.6 \times 10^{-4} - 2.8 \times 10^{-84}$ for V to soft X-ray band) which occurs by chance. This can be seen clearly in Fig. 4 from top to bottom for soft X-ray to V band. Details about the method of estimating correlation coefficient and probability are described in Pal et al. (2017a).

We computed the possible lag/lead between soft band and hard X-ray light curves. There are publicly available codes such as JAVELIN (Zu et al. 2011, 2013) and Z-transformed discrete cross-correlation function (ZDCF) (Alexander 1997) which are capable of finding the presence/absence of any timing information between the light curves. JAVELIN software is based on damped random

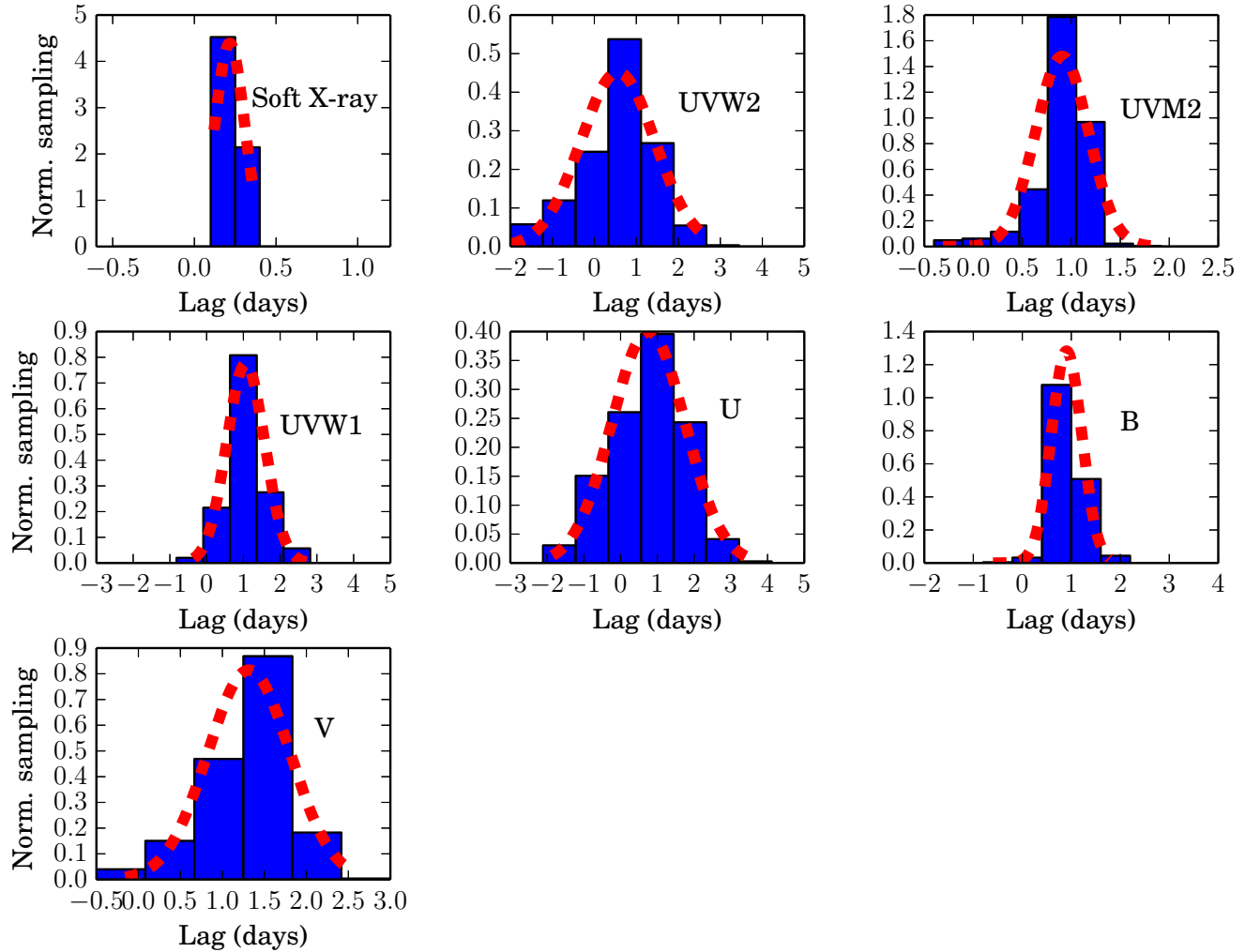


Figure 5. Probability distribution of lags for soft bands with respect to 1.5-10 keV band by using `JAVELIN` code. The dashed-red curve in each panel shows the Gaussian representation of probability distribution of the observed lag.

walk process which has been commonly found in quasar variability. This phenomenon was first introduced by Kelly et al. (2009). Since then, it has been used to understand the observed variability in the UV/optical bands (Kozłowski et al. 2010; MacLeod et al. 2010; Zu et al. 2011, 2013). We applied this software by assuming hard X-ray band as the first light curve and the soft bands as the second light curve to determine the lag distribution. The lag distribution between soft bands and hard X-ray band are shown in Fig. 5. Assuming Gaussian distribution, we estimated lags for soft bands with respect to hard X-ray band and found to be for soft X-ray band -0.22 ± 0.09 days, UVW2 band -0.56 ± 0.88 days, UVM2 band -0.91 ± 0.27 days, UVW1 band -1.1 ± 0.5 days, U band -0.76 ± 1.0 days, B band -0.9 ± 0.3 days and V band -1.3 ± 0.5 days.

We also applied `ZDCF` to assess the presence of time delay between the soft bands and the hard X-ray band. We run the package with minimum eleven data points, which have non-zero lag, along with non-uniform binning between a pair of bands to determine the cross-correlation function (CCF). We also derived the auto-correlation function (ACF) for each band using minimum eleven data points with non-uniform binning. The resulted CCF and ACF are displayed in the right and left panels of Fig. 6, respectively. The

ACF of each UV/optical band appears broader compared to the X-ray bands. The CCF of soft bands also show broader distribution towards the positive lag. This implies that the longer wavelength is delayed with respect to the hard X-ray band. We, therefore, estimated the lag of soft bands compared to the hard X-ray band by using `PLIKE` software provided by Alexander (1997). To quantify lags between soft bands and hard X-ray band, we considered CCF for all the soft bands in the range of -2 to 6 days. Following this procedure, the lags are determined to be – for soft X-ray band $-0.11^{+0.22}_{-0.14}$ days, UVW2 band $-0.36^{+0.48}_{-0.19}$ days, UVM2 band $-0.38^{+0.60}_{-0.13}$ days, UVW1 band $-1.41^{+0.48}_{-0.95}$ days, U band $-1.94^{+0.11}_{-0.75}$ days, B band $-1.62^{+0.21}_{-0.51}$ days and V band $-1.14^{+2.45}_{-0.84}$ days with respect to the hard X-ray band. The estimated lags by using `ZDCF` are found to be comparable to that of by using `JAVELIN` software.

3.3 Modeling of time lag spectrum

The central wavelength for each UV/optical band is considered as the mid-point between the wavelengths at half-maximum and is taken from Poole et al. (2008). The soft X-ray and hard X-ray bands are expressed in terms of corresponding central wavelengths

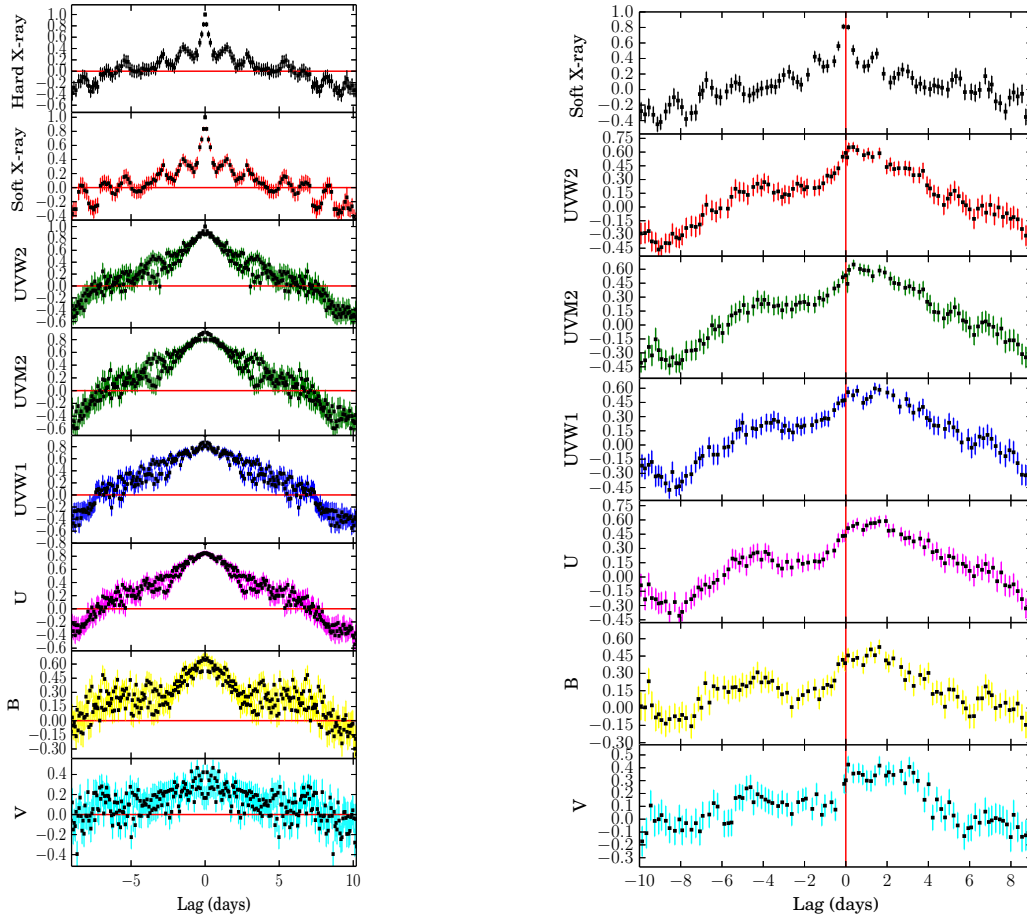


Figure 6. Left panel: From top to bottom- auto correlation function (ACF) of hard X-ray to UV/optical light curves using ZDCF function. Right panel: From top to bottom- the cross-correlation function (CCF) for the soft X-ray and each UV/optical bands compared to 1.5 – 10 keVband. The vertical solid line in the right panels represents zero delay.

as 2.5 ± 1.7 nm and 0.48 ± 0.35 nm, respectively. The derived lags by using ZDCF and JAVELIN softwares for the soft X-ray, UVW2, UVM2, UVW1, U, B and V bands are comparable. The lags, determined by ZDCF, were used to create the lag spectrum where lag is a function of wavelength. The derived lag spectrum is shown in Fig. 7.

3.3.1 Power law model

Power law model, normally used for thin disc, is expressed as

$$\tau = \alpha \left[\left(\frac{\lambda}{\lambda_0} \right)^\beta - 1 \right] \quad (1)$$

where τ , α , β are time delay for a central wavelength λ , power-law normalization and power-law index, respectively. Here, λ_0 is considered as a reference wavelength. According to the standard disc model, the time lag varies with 4/3rd power of wavelength. Here, we used the central wavelength of hard X-ray band ($\lambda_0 = 0.475$ nm) as the reference wavelength. We modeled the measured lag spectrum with power law model (Eq. 1) by allowing normalization and index to vary (see Eq. 1). In our fitting, as the power-law index was not well constrained, we fixed the index

at 4/3. The best-fit model was found to be $\tau = (2.01 \pm 0.28) \times 10^{-4} \left[\left(\frac{\lambda}{0.475} \right)^{4/3} - 1 \right]$ with statistics $\chi^2_{\nu}/dof = 0.85/6$.

3.3.2 Shakura-Sunyaev accretion disc model

In the lamppost geometry, the X-ray source is assumed to be at a height h above the disc in the vicinity of the SMBH. Radiation from the X-ray source gets absorbed in the disc which then re-emitted in longer wavelengths i.e., UV and optical bands. Thus, the thermal emission and the X-ray reprocessed emission from the disc increase the temperature of the disc at a given radius r . The following expression includes both these components to give a net temperature $T(r)$ at a radius r (Cackett et al. 2007; Berkley et al. 2000).

$$T(r) = \left(\frac{3GM\dot{M}}{8\pi\sigma r^3} \left(1 - \frac{r_{in}}{r}\right)^{1/2} + \frac{(1-A)L_x}{4\pi\sigma r_x^2} \cos(\theta_x) \right)^{1/4} \quad (2)$$

where M , G , \dot{M} , r_{in} , r_x , L_x and A are the black hole mass, gravitational constant, the mass accretion rate, radius of the innermost stable orbit and the distance of the disc element (i.e., annulus ring) from the X-ray source, luminosity of the source and albedo for X-ray heating, respectively. The term θ_x stands for the angle between

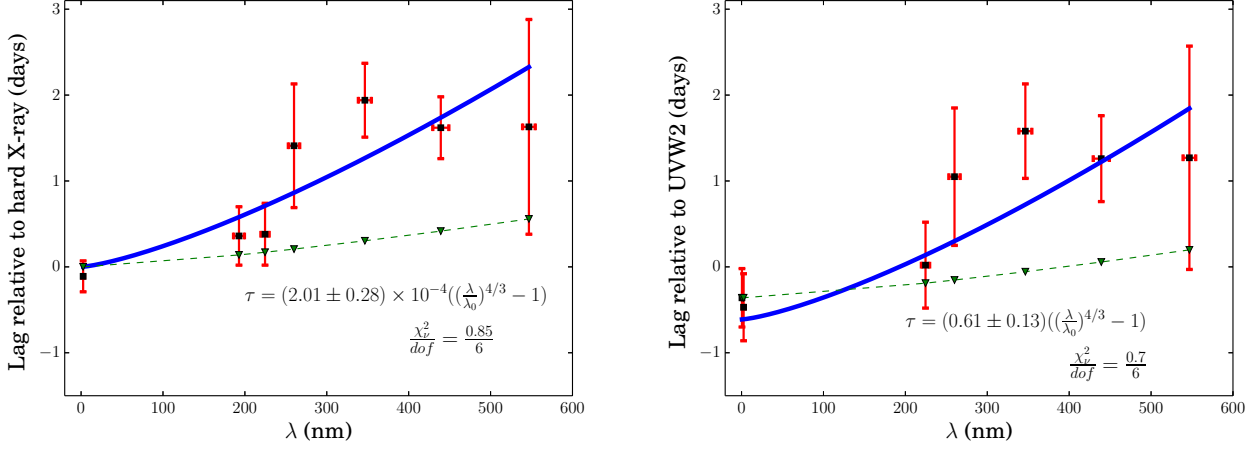


Figure 7. Left panel: The lag spectrum with respect to the hard X-ray band. The fit for the lag spectrum (a) Blue curve- the best-fit power law model ($2.0 \pm 0.3 \times 10^{-4} [(\lambda/0.475)^{4/3} - 1]$). (b) Green dashed curve : standard accretion thin disc theoretical model. Right panel: The lag spectrum with respect to the UVW2 band. The fit for the lag spectrum (a) Blue curve- the best-fit power law model ($0.6 \pm 0.1 \times 10^{-4} [(\lambda/0.475)^{4/3} - 1]$). (b) Green dashed curve : standard accretion thin disc theoretical model for NGC 4593. Clearly, the larger lag of U band suggests an extra component of emission possibly emission from broad line region.

the normal to the annulus ring of the disc and the line connecting to the annulus ring and the X-ray source. Cosine of θ_x and r_x can be expressed as $\frac{h}{r_x}$ and $(h^2 + r^2)^{1/2}$, respectively. Assuming height h and inner radius r_{in} to be very small compared to radius r , $\frac{\cos(\theta_x)}{r_x}$ and $(1 - \frac{r_{in}}{r})^{1/2}$ in Eq. 2 approximately become $\sim \frac{h}{r^3}$ and ~ 1 , respectively. r can be represented in terms of $T(r)$, M , \dot{M} , h , A and L_x . Using Wein's law, temperature $T(r)$ takes the form into the wavelength, r can be expressed as a function of wavelength. Then, r can be written as a product of time delay τ and light speed c . Thus, for a given reference wavelength λ_0 , delay τ can be expressed as

$$\tau - \tau_0 = \left(\frac{1}{c}\right) \left(\frac{\lambda_0}{k}\right)^{4/3} \left(\frac{3GM\dot{M}}{8\pi\sigma} + \frac{(1-A)L_x h}{4\pi\sigma}\right)^{1/3} \left[\left(\frac{\lambda}{\lambda_0}\right)^{4/3} - 1\right]. \quad (3)$$

where k is 2.9×10^6 nm K.

Eq. 3 allows to estimate the lags based on the standard disc theory. We used $M = 1 \times 10^7 M_\odot$ (Denney et al. 2006), $h = 6r_g$ and $r_{in} = 6r_g$ and $A = 0.2$. The mass accretion rate in the unit of Eddington mass accretion rate $\dot{m}_E (= \frac{\dot{M}}{M_E}) = 0.04$ and luminosity $L_x = 10^{43.7}$ erg s^{-1} were also used required to estimate the lags (Vasudevan & Fabian 2009). The lag τ_0 corresponding to the reference wavelength λ_0 would be zero day in the lag calculation from the standard accretion disc model. The theoretically predicted lags are shown as green dashed line in Fig. 7. The filled triangles on the predicted lag curve correspond to the effective wavelength of the respective band. Thus, the observed lags, marked as filled squares in the figure, are found to be longer than the estimated lags from the Shakura-Sunyaev disc model.

Assuming face-on accretion disc, the normalization can provide a rough estimate to the size of emitting region of the reference wavelength (e.g., Edelson et al. 2015). In our case, we assumed the hard X-ray as the reference wavelength. We, therefore, can estimate the size of the X-ray emitting region. Using the best-fit value

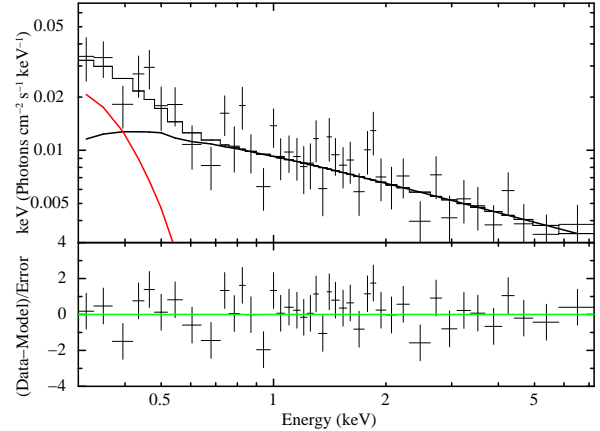


Figure 8. 00092353119: The best-fit model, data and residuals in σ are displayed here. The red solid curve represents the blackbody component used for describing the soft X-ray excess and black solid line exhibits the power-law continuum model.

of $\alpha = 2.01 \pm 0.28 \times 10^{-4}$, the estimated size of the emitting region is $0.0002 \times 86400 \times 3 \times 10^5 \sim 10^7$ km. For a given mass of black hole M , the Schwarzschild radius is $R_S \sim 2.96(\frac{M}{M_\odot})$ km. Using the mass of NGC 4593 ($\sim 10^7 M_\odot$), the size of the regions is found to be $\sim 10^7$ km as expected. Similarly, the size of UVW2 region is found to be $\sim 530R_S$.

We summarize as follows: the power law model with 4/3rd power of wavelength, as expected from the standard disc, fits the observed lag spectrum. Using the available mass, accretion rate, bolometric luminosity and albedo, theoretically estimated lags are found to be smaller compared to the observed lags. For example, the predicted lag of B band is ~ 0.5 days whereas the observed lag of B band is ~ 1.6 days. This implies that the real accretion disc appears larger in size compared to the predicted size by the standard disc model.

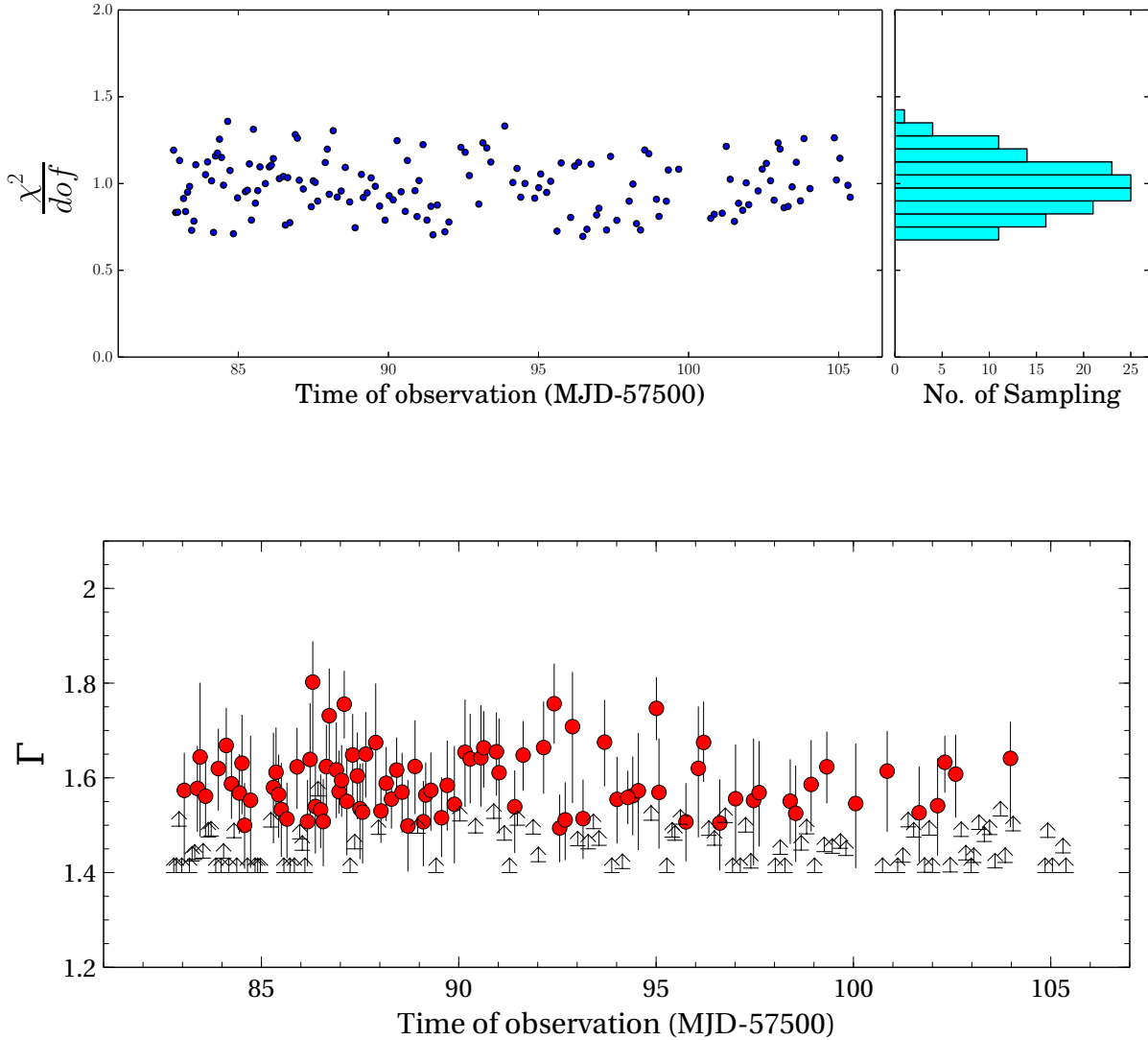


Figure 9. The reduced χ^2 squared in upper panel for each observation with its MJD. This clearly shows that simple powerlaw+blackbody model is an acceptable model to describe the X-ray band. The time variation of photon index Γ is shown in lower panel.

3.4 Spectral analysis

The *Swift*/XRT, which covers 0.3-10 keV energy range, is appropriate to study the presence of several spectral components such as primary power law continuum, soft X-ray excess and Fe-K α emission line along with the signature of absorption components in the soft band. Presence of soft X-ray excess and warm absorber have been detected in the galaxy NGC 4593 (Ursini et al. 2016; Ebrero et al. 2013). We used phenomenological models such as blackbody (*bbody* in *XSPEC*) for the soft X-ray excess and power law (*powerlaw* in *XSPEC*) continuum to describe the X-ray broadband spectra from all the observations used in the present work. We multiplied photo-absorption model (*phabs* in *XSPEC*) to modify the soft X-ray band due to the Galactic absorption. Thus, we used *phabs(bbody+powerlaw)* model to fit spectra from all the observations except those which were highly piled-up. We found that this composite model is sufficient to describe the broad-band spec-

trum of NGC 4593 without any requirement of warm absorber or Fe-K α emission line. A representative spectrum of the galaxy (Obs. ID-00092353119) is shown in Fig. 8 along with the best-fit model components and residuals obtained from our fitting. The distribution of reduced χ^2 values obtained from the spectral fitting of all the observations used in present work is displayed in upper panel of Fig. 9. We obtained similar correlation between the fluxes of soft X-ray excess and power law continuum as we found in the count-count plot as shown in Fig. 4(a). We could not constrained the power-law photon index for all the observations due to low exposure. The lower panel of Fig. 9 shows the variation of the power-law photon index Γ over the observation campaign and found to be consistent as reported in Ursini et al. (2016).

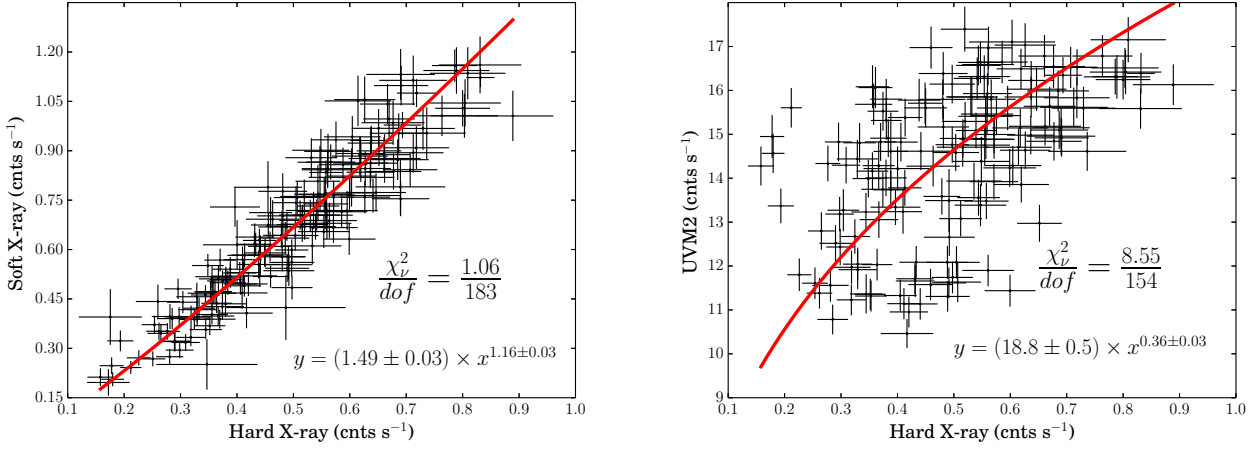


Figure 10. Count–count plots for the soft X–ray and hard X–ray (left panel), and the UVM2 and hard X–ray (right panel) bands are shown for the modeling with a power law $y = (1.49 \pm 0.03) \times x^{1.16 \pm 0.03}$ and $y = (18.8 \pm 0.5) \times x^{0.36 \pm 0.03}$, respectively.

4 DISCUSSION

We analyzed the variability observed in the UV/optical and X-ray bands of a Seyfert 1 galaxy NGC 4593 using archival intensive *Swift* campaign during July 13 – August 5, 2016. We applied various tools to investigate variability seen the UV/optical and X-ray light curves. Linear correlation between the 1.5 – 10 keV and one of the low energy i.e., the UV/optical bands including soft X-ray band was used in our work. We studied the count-count correlation with positive offset (C3PO) method to distinguish less variable component compared to X-ray emission. Cross-correlation analysis was done using ZDCF and JAVELIN and derived the lags for the soft bands compared to hard X-ray band. We summarize our main results which are as follows:

- (i) NGC 4593 exhibited strong variability in all bands on short and long timescales.
- (ii) The linear fit to the correlation between the hardness ratio and the hard X-ray count rate (see Fig. 3) suggests that the source retains its nature of being softer when brighter as found by Ursini et al. (2016).
- (iii) The negative offset from C3PO technique favors a weakly absorbed soft X-ray band and is consistent as found by Ursini et al. (2016). The positive offset in linear fit for the UV/optical emission also suggests the presence of weakly variable component in the UV/optical bands possibly the disc emission (see Fig. 4).
- (iv) Linear correlation coefficient ($\rho = 0.29 - 0.94$) and low p value ($10^{-4} - 10^{-84}$) infer that the observed light curves in the UV/optical bands are strongly correlated with the hard X-ray light curve.
- (v) The UV/optical emission follow the hard X-ray emission by $\sim 0.4 - 1.5$ days as estimated by the cross-correlation analysis. The lag estimated for each pair of light curves by both ZDCF and JAVELIN are found to be comparable.
- (vi) The observed lag increases with wavelength despite large errors. The power law model with 4/3rd power of wavelength describes well to the observed lag spectrum (lag vs. wavelength).
- (vii) The observed lags are found to be larger than the derived lags from Shakura-Sunyaev disc theory after adding both the thermal and X-ray heating (see Fig. 7).

The observed light curves in the X-ray as well as UV/optical

bands appear highly variable on both long and short timescales. The X-ray emission varies by a factor of ~ 5 and the UV/optical emission vary by $\sim 80-20\%$ over about a month timescale. The X-ray emission fluctuates rapidly by a factor of ~ 2 while the UV/optical emission vary slowly ($\sim 27-18\%$). Such observed variations may be associated with various phenomena such as extinction/absorption along the line of sight, the changes in the accretion flow, Comptonization of seed photons in the disc and X-ray reprocessing in the accretion disc. The hardness ratio (right bottom panel of Fig 2) and positive offset in the linear fit (Fig. 4) imply that there is no significant effect of absorption/extinction on the emission on a month timescale. The observed variation in hardness ratio on hours time scale (right bottom panel of Fig 2) indicates the presence of variable absorption in the galaxy. Similarly, from the count-count correlations (Fig 4), scatter of data points from the linear fit in UV/optical bands also suggests the possible presence of absorption.

A careful investigation of the scatters suggests that the distribution of data points in count-count correlation plots (Fig 4) follows a non-linear trend (except soft X-ray band and V band). This indicates that the variability observed in above bands may be due to absorption along the line of sight. For example, the negative offset in soft X-ray band can be verified by assuming that both soft and hard X-ray bands are affected by absorption. If that is the case, the simple power law continuum model can be modified by incorporating absorption component. This implies, in soft X-ray band, the observed count rate $S(t)$ at energy E_S can be expressed as:

$$S(t) = \left(\left\{ \prod_{i=1}^N \exp[-N_{H,i}(t)\sigma(E_S)] \right\} C E_S^{-\Gamma} \right), \quad (4)$$

where N is the number of obscuring clouds along the line of sight with variable equivalent hydrogen column density $N_{H,i}(t)$. We also assume that the shape of the X-ray continuum remains constant. $\sigma(E_S)$ and C are the photo-electric cross-section in soft energy band and normalization constant, respectively. The above equation can be rewritten as,

$$S(t) = \exp \left\{ \left[- \sum_{i=1}^N N_{H,i}(t) \right] \sigma(E_S) \right\} C E_S^{-\Gamma}, \quad (5)$$

and similarly the same will be the case for the count rate in hard X-ray band at energy E_H ,

$$H(t) = \exp \left\{ \left[- \sum_{i=1}^N N_{H,i}(t) \right] \sigma(E_H) \right\} C E_H^{-\Gamma}. \quad (6)$$

We can rewrite above equations by eliminating $[- \sum N_{H,i}(t)]$ to get the following expression between the count rates in the two bands,

$$S = A H^\beta, \quad (7)$$

where A is another normalization constant and slope β is described as $\beta = \sigma(E_S)/\sigma(E_H)$. Eq. 7 predicts a non linear relation between hard and soft bands. Even if number of clouds N changes with time, Eq. 7 should be valid.

We used Eq. 7 to test the absorption (irrespective of either warm absorption or neutral) in the soft and hard X-ray bands. We modeled the count-count correlation assuming soft X-ray counts as the function of hard X-ray counts and obtained a marginal improvement compared to the earlier linear fit. It is interesting to note that the slope of the power law fit (~ 1.16 , as shown in left panel of Fig. 10) is consistent with the photo-absorption cross-section dependency on energy ($\sigma \propto E^{-3}$). This suggests that the soft X-ray band is mildly affected from absorption, supporting the negative offset finding in count-count correlation study.

It is interesting to check similar effect in the UV/optical bands where we noticed non-linear trends. We modeled the count-count correlation between the UVM2 band (as the soft band) and the hard X-ray band and presented in the right panel of Fig. 10. We found significant improvement ($\frac{\chi^2}{dof} = 1316.7/154$) in statistics compared to the linear fit ($\frac{\chi^2}{dof} = 1336.4/154$). Interestingly, the slope $\beta \sim 0.36$ was found to be lesser than one. This implies that the photo-absorption cross-section is higher in the hard X-ray band compared to the UVM2 band. Similar fits were also found in other UV/optical bands. Such findings are contrary to the theory of photo-absorption where photo-absorption cross section $\sigma \propto E^{-3}$. This suggests that the scatters present in the UV/optical bands are not caused due to the line of sight absorption. These scatters may be due to diffused emission from broad-line regions.

On the other hand, strong correlation between the soft bands and the hard X-ray band infers that these emission are related to either changes in the accretion flow, Comptonization phenomena or X-ray reprocessing. A month timescale is too short to see any significant variation caused by the changes in the accretion flow as the expected timescale of fluctuations in the accretion flow is $\sim 10^3$ years or more (Smith & Vaughan 2007; Pal et al. 2017b). The observed short timescale variation can be caused by either inverse Comptonization or the X-ray reprocessing phenomenon in the disc. In the inverse Comptonization process, the variations in the UV/optical emission should lead the variations in the X-ray emission on the light-crossing timescale. Similarly, the X-ray reprocessing causes the short timescale in such a way that the changes in the UV/optical emission lags the fluctuations observed in the X-ray emission.

Cross-correlation analysis using ZDCF shows that the observed changes in the UV/optical bands lags the observed variations in the X-ray bands on short timescale of few days ($\sim 0.4 - 1.5$ days). Thus the inverse Comptonization process may not be working between the various bands. This implies that X-ray reprocessing is playing a major role to drive the observed variations on short timescale of few days ($\sim 0.4 - 1.5$ days). Such lags are very important and interesting to study various regions of the accretion disc

and its coupling with the X-ray corona. The lags provide the distribution of regions on the accretion disc which emit at various wavelengths. The observed lag as a function of wavelength is well described by 4/3rd power of the wavelength. This power law description of the lag spectrum is consistent with the standard accretion disc model (see blue curve in Fig. 7). However, the estimated lags from the Shakura-Sunyaev accretion disc theory under lamp-post geometry assumption appear smaller than the observed lags (see green dashed line in Fig. 7). For example, UVW1, U and B bands show clear longer lags than that of the predicted values from standard disc model while for Soft X-ray, UVW2, UVM2 and V bands, both the values marginally agree. Though, the estimated lags are determined by considering wavelength calculated from Wein's law, such assumption provides overestimation of lags by not including the geometrical effects (e.g., flux weighted mean radius, inclination) as presented in McHardy et al. (2014). By adding geometrical effects, the predicted lags would be further shortened.

From the observed time lag, the size of the disc is found to be larger compared to the standard disc prediction. There is a chance that the standard disc prediction might be underestimated due to the assumptions such as the disc is (i) optically thick and behaves like a blackbody and (ii) geometrically thin i.e. height to radius ratio is very small. In addition to above assumptions, in lamp-post geometry, the isotropically emitting corona is in compact form and lies on the spin axis of black hole. However, actual geometry of the disc and corona may be different. The disc may be a flared disc (e.g., Cunningham 1976) and the corona may be in extended form (e.g., Pal & Dewangan 2013; Kotov et al. 2001; Ingram & Done 2012). Figure 1 of Gardner & Done (2017) shows that if the extended corona illuminates the disc, such illumination can make the disc a flared disc. In that case, the wavelength dependent lag follows $\lambda^{7/3}$ profile rather than the $\lambda^{4/3}$ profile. This implies the observed lag may be due to enhanced flux from the outer disc region. Gardner & Done (2017) reported that the observed variation in UV/optical emission from NGC 5548 is not consistent with the reprocessing of hard X-rays rather it is due to the reprocessing of FUV emission from the inner region. Similar results were also reported in NGC 4151 (Edelson et al. 2017). Mathur et al. (2017) did not find any correlation between the continuum flux and emission line flux from *Chandra* and *Swift* observations of NGC 5548. They suggested that such anomaly is possibly caused due to the presence of warm Comptonizing medium in the inner disc which is consistent with the scenario given by Gardner & Done (2017). We also tried to investigate the possibility of second reprocessor by excluding the X-ray lags with respect to the UVW2 band. However, our results are not consistent with the possibility of second reprocessor (see right panel Fig. 7).

The findings presented in this paper are interesting in a sense that our knowledge of real accretion theory is not complete and the actual accretion disc appears larger in size than that predicted by standard disc model. In addition to the lag-wavelength profile of $\lambda^{4/3}$, we found larger lag in the U band. This suggests an additional component of emission contributing in this band. This emission component may be diffused emission from broad line region. The nature of real accretion disc could be very complex and may provide longer lag due to its inhomogeneity of the outer surface and warped nature (Dexter & Agol 2011). The micro-lensing results also suggest that the observed emission requires larger region of the outer accretion disc over standard accretion disc (Morgan et al. 2010). The power-law index was fixed at 4/3 in our analysis due to the fact that this parameter is not well constrained given the available data. In addition, the large errors in the lag estimation can be

improved by having more observations of the source. However, better estimation of lag alone is not sufficient to constrain the physical size of the accretion disc in AGN. Along with the estimated lag, results from the effect of general relativity, geometrical effects, complex absorption near the accretion disc and disc-corona interaction together can provide reliable estimation of the disc size.

5 ACKNOWLEDGMENT

We sincerely thank the reviewer for his/her useful comments and suggestions which improved the paper significantly. The High Energy Astrophysics Science Archive Research Center (HEASARC) of the NASA/GSFC Astrophysics Science Division and Smithsonian Astrophysical Observatory's High Energy Astrophysics Division were used for their available softwares and online webtools. This research has made use of the archival observations of *Swift* observatory and XRT Data Analysis Software (XRTDAS) developed under the responsibility of the ASI Science Data Center (ASDC), Italy.

REFERENCES

- Alexander T., 1997, in *Astrophysics and Space Science Library*, Vol. 218, *Astronomical Time Series*, Maoz D., Sternberg A., Leibowitz E. M., eds., p. 163
- Arévalo P., Uttley P., Kaspi S., Breedt E., Lira P., McHardy I. M., 2008, *MNRAS*, 389, 1479
- Arévalo P., Uttley P., Lira P., Breedt E., McHardy I. M., Churazov E., 2009, *MNRAS*, 397, 2004
- Berkley A. J., Kazanas D., Ozik J., 2000, *ApJ*, 535, 712
- Boller T., Brandt W. N., Fink H., 1996, *A&A*, 305, 53
- Breedt E. et al., 2010, *MNRAS*, 403, 605
- Brenneman L. W., Reynolds C. S., Wilms J., Kaiser M. E., 2007, *ApJ*, 666, 817
- Buisson D. J. K., Lohfink A. M., Alston W. N., Fabian A. C., 2017, *MNRAS*, 464, 3194
- Burrows D. N. et al., 2005, *SSRv*, 120, 165
- Cackett E. M., Horne K., Winkler H., 2007, *MNRAS*, 380, 669
- Churazov E., Gilfanov M., Revnivtsev M., 2001, *MNRAS*, 321, 759
- Collier S., Horne K., Wanders I., Peterson B. M., 1999, *MNRAS*, 302, L24
- Connolly S. D., McHardy I. M., Skipper C. J., Emmanoulopoulos D., 2016, *MNRAS*, 459, 3963
- Cunningham C., 1976, *ApJ*, 208, 534
- Denney K. D. et al., 2006, *ApJ*, 653, 152
- Dexter J., Agol E., 2011, *ApJ*, 727, L24
- Ebrero J., Kaastra J. S., Kriss G. A., de Vries C. P., Costantini E., 2013, *MNRAS*, 435, 3028
- Edelson R. et al., 2017, *ApJ*, 840, 41
- Edelson R. et al., 2015, *ApJ*, 806, 129
- Evans P. A. et al., 2009, *MNRAS*, 397, 1177
- Evans P. A. et al., 2007, *A&A*, 469, 379
- Fausnaugh M. M. et al., 2016, *ApJ*, 821, 56
- Gardner E., Done C., 2017, *MNRAS*, 470, 3591
- Gaskell C. M., 2008, in *Revista Mexicana de Astronomia y Astrofisica Conference Series*, Vol. 32, *Revista Mexicana de Astronomia y Astrofisica Conference Series*, pp. 1–11
- Gebhardt K. et al., 2000, *ApJ*, 543, L5
- Haardt F., Maraschi L., 1991, *ApJ*, 380, L51
- Ingram A., Done C., 2012, *MNRAS*, 419, 2369
- Kelly B. C., Bechtold J., Siemiginowska A., 2009, *ApJ*, 698, 895
- Koratkar A., Blaes O., 1999, *PASP*, 111, 1
- Kotov O., Churazov E., Gilfanov M., 2001, *MNRAS*, 327, 799
- Kozłowski S. et al., 2010, *ApJ*, 708, 927
- Krolik J. H., Horne K., Kallman T. R., Malkan M. A., Edelson R. A., Kriss G. A., 1991, *ApJ*, 371, 541
- Leighly K. M., 1999, *ApJS*, 125, 317
- Lobban A., Porquet D., Reeves J., Markowitz A., Nardini E., Grosso N., 2017, *ArXiv e-prints*
- MacLeod C. L. et al., 2010, *ApJ*, 721, 1014
- Maoz D., Markowitz A., Edelson R., Nandra K., 2002, *aj*, 124, 1988
- Markowitz A. G., Reeves J. N., 2009, *ApJ*, 705, 496
- Marshall K., Ryle W. T., Miller H. R., 2008, *ApJ*, 677, 880
- Mathur S. et al., 2017, *ApJ*, 846, 55
- McHardy I. M. et al., 2014, *MNRAS*, 444, 1469
- McHardy I. M. et al., 2016, *Astronomische Nachrichten*, 337, 500
- Mehdipour M. et al., 2011, *A&A*, 534, A39
- Morgan C. W., Kochanek C. S., Morgan N. D., Falco E. E., 2010, *ApJ*, 712, 1129
- Nandra K., Clavel J., Edelson R. A., George I. M., Malkan M. A., Mushotzky R. F., Peterson B. M., Turner T. J., 1998, *ApJ*, 505, 594
- Noda H., Makishima K., Nakazawa K., Uchiyama H., Yamada S., Sakurai S., 2013a, *PASJ*, 65
- Noda H., Makishima K., Nakazawa K., Yamada S., 2013b, *ApJ*, 771, 100
- Noda H., Makishima K., Yamada S., Torii S., Sakurai S., Nakazawa K., 2011, *PASJ*, 63, S925
- Noda H. et al., 2016, *ApJ*, 828, 78
- Onken C. A., Peterson B. M., Dietrich M., Robinson A., Salamanca I. M., 2003, *ApJ*, 585, 121
- Pal M., Dewangan G. C., 2013, *MNRAS*, 435, 1287
- Pal M., Dewangan G. C., Connolly S. D., Misra R., 2017a, *MNRAS*, 466, 1777
- Pal M., Dewangan G. C., Kembhavi A. K., Misra R., Naik S., 2017b, *ArXiv e-prints*
- Pal M., Dewangan G. C., Misra R., Pawar P. K., 2016, *MNRAS*, 457, 875
- Peterson B. M. et al., 2004, *ApJ*, 613, 682
- Poole T. S. et al., 2008, *MNRAS*, 383, 627
- Reynolds C. S., Brenneman L. W., Wilms J., Kaiser M. E., 2004, *MNRAS*, 352, 205
- Roming P. W. A. et al., 2005, *SSRv*, 120, 95
- Santos-Lleo M., Clavel J., Barr P., Glass I. S., Pelat D., Peterson B. M., Reichert G., 1995, *MNRAS*, 274, 1
- Shakura N. I., Sunyaev R. A., 1973, *A&A*, 24, 337
- Shappee B. J. et al., 2014, *ApJ*, 788, 48
- Smith R., Vaughan S., 2007, *MNRAS*, 375, 1479
- Starkey D. et al., 2017, *ApJ*, 835, 65
- Strauss M. A., Huchra J. P., Davis M., Yahil A., Fisher K. B., Tonry J., 1992, *ApJS*, 83, 29
- Sunyaev R. A., Titarchuk L. G., 1980, *A&A*, 86, 121
- Taylor R. D., Uttley P., McHardy I. M., 2003, *MNRAS*, 342, L31
- Troyer J., Starkey D., Cackett E. M., Bentz M. C., Goad M. R., Horne K., Seals J. E., 2016, *MNRAS*, 456, 4040
- Ursini F. et al., 2016, *MNRAS*, 463, 382
- Vanden Berk D. E. et al., 2001, *aj*, 122, 549
- Vasudevan R. V., Fabian A. C., 2009, *MNRAS*, 392, 1124
- Yuan F., Narayan R., 2014, *ARAA*, 52, 529

Zu Y., Kochanek C. S., Kozłowski S., Udalski A., 2013, ApJ, 765,
106
Zu Y., Kochanek C. S., Peterson B. M., 2011, ApJ, 735, 80